

Mid-infrared photoacoustic spectroscopy based on ultrasound detection for blood component analysis

RYOTA SASAKI, SAIKO KINO, AND YUJI MATSUURA* 

Graduate School of Biomedical Engineering, Tohoku University, 6-6-05 Aoba, Sendai, 980-8579, Japan

**yuji.matsuura.c1@tohoku.ac.jp*

Abstract: For the non-invasive measurement of biological tissue, a piezoelectric photoacoustic spectroscopy (PZT-PAS) system that detects a single frequency of ultrasound induced by the irradiation of pulse-modulated mid-infrared laser light was developed. PA spectra of the optical phantom and biological samples were obtained, and the relationship between the PA signal intensity and optical absorbance in the fingerprint region ($930\text{--}1,200\text{ cm}^{-1}$) was analyzed to estimate the optical absorbance. The resonance vibration of the induced ultrasound was utilized to further increase the signal strength for biological tissue measurement. Consequently, PA spectrum reflecting the absorption of components in biological tissues was obtained.

© 2023 Optica Publishing Group under the terms of the [Optica Open Access Publishing Agreement](#)

1. Introduction

With the global increase in the number of patients with diabetes, daily blood glucose measurements have become necessary [1]. Although self-monitoring of blood glucose devices are already on the market, the blood sampling of these devices require skin puncture, causing pain and infection risks to users [2]. Therefore, a noninvasive monitoring system that can easily measure blood components from the skin surface is required.

Many attempts based on optical approaches have been reported to achieve non-invasive glucose detection and/or measurements [3,4], including fluorescence techniques [5], Raman spectroscopy [6], and infrared spectroscopy [7]. Infrared spectroscopy can be divided into near-infrared spectroscopy and mid-infrared spectroscopy, depending on the wavelength of the light. Some affordable and compact systems have been proposed based on near-infrared spectroscopy because there are multiple choices of light sources and detectors [8,9]. However, the measurement accuracy in the near-infrared region is limited because the optical absorption that can be detected in the near-infrared region is an overtone of fundamental molecular vibrations in the mid-infrared region. Furthermore, they are superimposed in the near-infrared region, making it difficult to distinguish each component. However, mid-infrared spectroscopy based on a wavelength range of $3\text{--}12\text{ }\mu\text{m}$ enables the detection of strong and isolated absorption peaks derived from fundamental molecular vibrations, including the fingerprint region ($8\text{--}10\text{ }\mu\text{m}$) of biological tissue [10]. For these uses, the attenuated total reflection (ATR) method utilizing an evanescent wave on the boundary between a sample and an ATR prism has been widely used [11–13]. This method can detect plasma components in the interstitial fluid (ISF), and the glucose concentration in the ISF reflects the blood glucose level [14], so that it enables non-invasive glucose measurement. However, the measurable parts of the human body are limited to those that do not have a stratum corneum (SC), for example, lip mucosa [15], owing to the small penetration depth ($2\text{--}3\text{ }\mu\text{m}$) of evanescent waves.

Another method, mid-infrared spectroscopy with photoacoustic detection, has become popular. With this method, photoacoustic spectroscopy (PAS), the heat generated by the absorption of the excitation light, causes the medium to expand and contract periodically, and the acoustic waves generated by these periodic expansions and contractions are detected by acoustic or pressure

sensors. PAS is an attractive technique for the study of biological samples because it has the advantages of a simple system configuration. In addition, using the absorption coefficient of water of 817 cm^{-1} [16], the light penetration depth is calculated as approximately $25\text{ }\mu\text{m}$ [17], which is ten times deeper than the ATR method (Fig. 1). Consequently, it is expected to reach epidermis, enabling the measurement of blood components from human skin with SC.

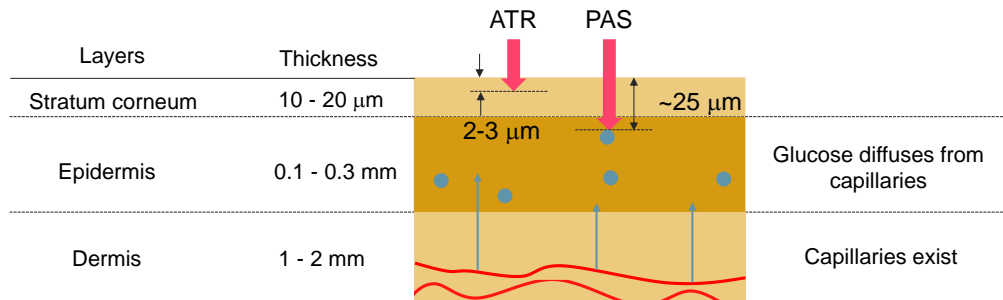


Fig. 1. Schematic of human skin and comparison of expected penetration depth for ATR spectroscopy and PAS.

It has already been applied in bioanalysis by several authors. von Lilienfeld-Toal *et al.* first observed the correlation between blood sugar and photoacoustic signals by measuring the forearm of the human body [18]. They performed this study with two individual quantum cascade lasers (QCLs): $1,080\text{ cm}^{-1}$ for the glucose peak and $1,066\text{ cm}^{-1}$ for the background. Kottmann *et al.* published the next paper that sensed glucose in epidermal skin with a detection limit of 100 mg/dl [19]. Thereafter, they reported an improved correlation between invasive blood glucose data and photoacoustic (PA) signals ($r^2 = 0.8$) [20]. The measurement error was $\pm 30\text{ mg/dL}$ at a 90% confidence level, although the detection sensitivity can be improved.

All previous reports on noninvasive measurements selected the combination of a microphone and photoacoustic (PA) cell for signal detection. However, two main drawbacks of this microphone approach have been reported: background noise owing to increasing humidity inside the PA cell, and instability owing to temperature changes. The former occurs because of the absorption of mid-infrared light in water vapor generated by skin perspiration during measurement [21]. Although this problem can be solved by introducing a windowless PA cell [22], it may be necessary to increase the signal sensitivity by optimizing the PA cell configuration using the finite element method (FEM). The latter occurs when the pressure inside the PA cell varies with temperature, which causes fluctuations in the detected PA signal.

To solve these problems of the microphone-based PAS method, in this study, we propose a PAS system based on piezoelectric detection. In this system, ultrasound is generated by mid-infrared laser pulses with a repetition rate of several hundred kilohertz, and ultrasound propagating through biological tissue with small attenuation is detected by a lead zirconate titanate (PZT) transducer attached to the sample surface. This PZT-based PAS (PZT-PAS) system does not require a PA cell; therefore, there is no water vapor problem, and the PZT can be mounted at any position on the sample, contributing to a simpler system configuration. PZT-PAS has been applied in other fields, such as the analysis of semiconductors [23] and identification of chemical compounds [24]. However, applications for bioanalysis, particularly in combination with mid-infrared spectroscopy, have rarely been proposed. Therefore, to demonstrate the effectiveness of this system, we first presented the results of acquiring the PA spectra of an optical phantom and biological samples. The relationship between the PA signal intensity and optical absorbance in the mid-infrared region was analyzed by changing the glucose concentration in the optical phantom. To further enhance the signal strength, we proposed the use of resonance vibration

originating from ultrasonic standing waves in the sample and demonstrated their effectiveness through experiments on a human earlobe.

2. Methods

Figure 2 shows the schematic of the experimental setup. The mid-infrared laser beam from a tunable external cavity quantum cascade laser (EC-QCL) (Hedgehog, Daylight Solutions, USA) was focused on the sample by an off-axis parabolic mirror. This EC-QCL has a tuning range of $930 - 1,200 \text{ cm}^{-1}$, and emits laser pulses at a repetition frequency of 500 to 600 kHz and a pulse width of 100 ns. In our measurement system, the laser was pulse-modulated with a small duty ratio of approximately 5% to increase the peak power of the laser pulses, thereby improving the signal-to-noise ratio (SNR) obtained. These results were confirmed both experimentally and theoretically. The pulse energy was $0.024 \mu\text{J}$ when the average output power was 12.2 mW, the repetition rate was 500 kHz, and the beam size was approximately 2 mm. Thus, the fluence was calculated to be as small as $7 \times 10^{-4} \text{ mJ/cm}^2$, which was below the maximum permissible exposure (MPE) [25]. The ultrasound induced in the sample by the laser pulses was detected by a piezoelectric (PZT) transducer (R-CAST AE Sensor M304 A, Fuji Ceramics, Japan) attached to the sample, and the signal was processed by a lock-in amplifier synchronized with the laser pulse. The PZT transducer had a resonant frequency of 300 kHz ($\pm 20\%$). The raw signal intensity spectrum was obtained from 930 to $1,200 \text{ cm}^{-1}$ with a 2 cm^{-1} step, and then the PA spectrum was obtained by normalizing it with the laser power spectrum measured by a laser power meter. All data shown in this paper are the average of four measurements. We chose this number of measurements considering the balance between the improvement of the SNR and instability caused by the increase of measurement time.

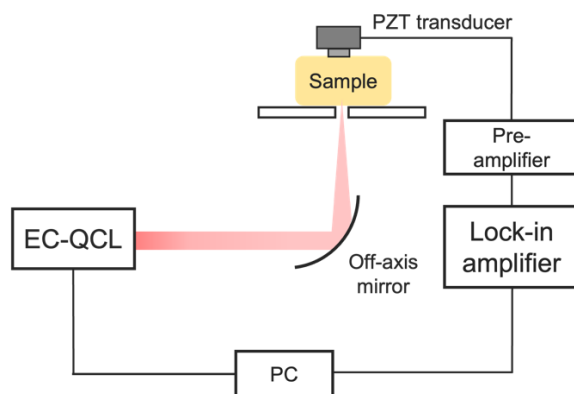


Fig. 2. Schematic of experimental setup.

Figure 3 shows the principle of our measurement method. The laser pulses from EC-QCL were absorbed by the target molecule of a sample and its light energy was converted to thermal energy. This thermal energy caused periodic expansions and contractions of the medium, resulting in the generation of PA waves. Here, the PA waves were in the ultrasound range because the repetition rate of the irradiation pulses was in the order of $\sim 10^2 \text{ kHz}$. The PA waves radially propagated and were detected by the PZT transducer.

In this study, an ATR spectroscopy system, including a zinc sulfide (ZnS) trapezoidal prism, hollow optical fiber and Fourier transform infrared spectrometer (FTIR) (Tensor 27, Bruker, Germany) [26] was also utilized to verify the feasibility of the proposed system. In ATR measurements, optical absorbance was measured with a frequency resolution of 2 cm^{-1} using air

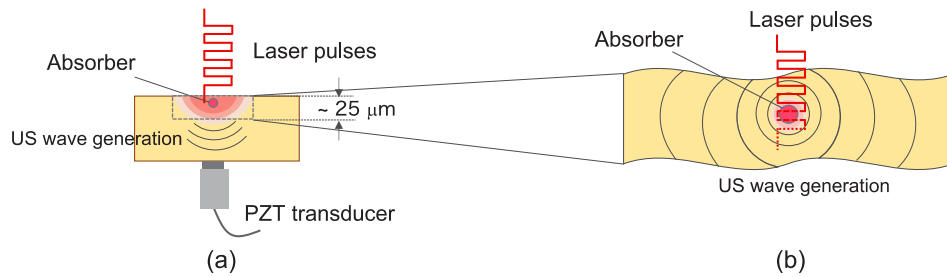


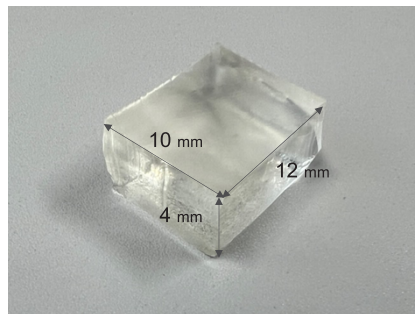
Fig. 3. Schematic of measurement principle.

as reference. The integration times of sample and reference were 128 and 32, respectively. All the ATR spectra depicted in the following section were obtained using this system.

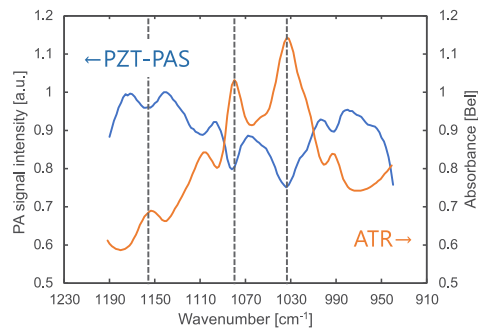
3. Results and discussion

3.1. Relationship between PA signal intensity and optical absorption

We first performed a feasibility study of piezoelectric detection in the mid-infrared region by comparing the obtained PA spectrum with the ATR spectrum. A 10% gelatin phantom (gelatin, Type A, Wako Pure Chemical, Japan), with 10% glucose (D(+)-Glucose, Wako Pure Chemical, Japan) whose appearance is shown in Fig. 4(a), was used for the sample. Figure 4(b) shows a comparison between the PA spectrum measured by the system shown in Fig. 2 and the optical absorption spectrum measured by the ATR spectroscopy system. In this measurement, the repetition frequency and pulse width of the EC-QCL were set to 500 kHz and 100 ns, respectively, and a PZT transducer was attached to the opposite side of the irradiation point.



(a)



(b)

Fig. 4. (a) Appearance of gelatin phantom and (b) PA spectrum and ATR spectrum of the gelatin phantom with 10% glucose.

Some spectral features of the PA spectrum matched with the ATR spectrum, such as the absorption peaks at $1,034\text{ cm}^{-1}$, $1,078\text{ cm}^{-1}$ and $1,155\text{ cm}^{-1}$. Because these peaks originated from the vibrations or bands of the glucose molecules [27,28], this result shows the potential use of spectral analysis with PZT-PAS in the mid-infrared region for glucose level measurements. However, the PA spectrum is almost inverted with respect to the ATR absorption spectrum. This phenomenon is different from the typical PA spectrum detected by microphones, whose intensity is proportional to the absorption. This is because the intensity of the generated ultrasonic

waves is nonlinear with respect to optical absorption. Jackson and Amer [29] theoretically showed that this occurs when optical absorption is extremely large. In their study, the signal detected by the PZT transducer was theoretically predicted by solving the thermoelastic equations using Green's functions for the stress. When the absorption is small, the irradiated light is entirely absorbed in the medium, to ensure that both surfaces of the medium stretch on average, originating from the thermal expansion of the central region, that is average expansion. Thus, the PA amplitude was proportional to the absorption. However, when the absorption is extremely large, the heated region is limited to the illuminated region of the sample surface; consequently, only the illuminated region stretches, and the other areas contracts, results in nonlinearity due to the competition [23]. In our case, the latter condition is considered to be applicable because the absorption of the phantom in the mid-infrared region is significantly large: the absorption coefficient of water is 817 cm^{-1} and this value is much larger than GaAs of $\sim 20 \text{ cm}^{-1}$ [30], which was analyzed in Ref. [23]. In addition, the pressure change caused by PA effect was 0.57 bar as calculated below, which does not cause noticeable deformation.

The temperature increases along the depth direction z of the sample caused by the absorption of one of the repeated light pulses is given as follows [31]:

$$\Delta T = \frac{(1 - R)\alpha F_0 e^{-\alpha z}}{\rho C}, \quad (1)$$

where R is the reflectance at the surface, α is the optical absorption coefficient, F_0 is the irradiation fluence, and ρC is the heat capacity per unit volume. When a laser beam with a repetition rate of 500 kHz and pulse width of 100 ns is irradiated on biological tissue, the temperature increase at the surface is estimated as $\Delta T = 0.114^\circ\text{C}$ using the refractive index $n = 1.35$, $\alpha = 817 \text{ cm}^{-1}$, and $\rho C = 3.47 \text{ J/}^\circ\text{C/cm}^3$ of water. Such minute changes in temperature cause no damage to biological tissues. Pressure generated by the heat increase [32] is expressed as

$$p = \Gamma \rho C \cdot \Delta T, \quad (2)$$

where Γ is the unitless Grüneisen coefficient. By setting $\Gamma = 0.12$, as in Ref. [33], the pressure obtained was $p = 0.57 \text{ bar}$. The detection of such extremely small pressure fluctuations was achieved by combining a highly sensitive PZT with a lock-in amplifier.

To assess the relationship between the PA signal intensity and optical absorption in our measurement region, $930\text{--}1,200 \text{ cm}^{-1}$, we prepared gelatin phantoms with different glucose concentrations from 2% to 10%, with increments of 2%, and obtained the PA and ATR spectra. Figure 5(a) shows the ATR spectra of the gelatin phantom with each glucose concentration. The absorbance at some observed absorption peaks, such as $1,034 \text{ cm}^{-1}$ and $1,078 \text{ cm}^{-1}$, increased as the glucose concentration increased. Figure 5(b) shows the calibration curve for the absorbance and glucose concentration at $1,034 \text{ cm}^{-1}$. As can be seen, there is a high linearity between them, which means that these data can be applied to analyze the relationship between optical absorption and PA signal intensity.

Figure 6(a) shows the PA spectra of gelatin phantoms with different glucose concentrations, and Fig. 6(b) shows the relationship between the optical absorption and PA signal intensity at $1,034 \text{ cm}^{-1}$. The horizontal axis shows absorbance at $1,034 \text{ cm}^{-1}$ measured using the ATR method, where an absorption peak of glucose was observed. The vertical axis is the corresponding PA signal intensity for each concentration. As shown in Fig. 6(b), the PA signal intensity exhibited linearity with a negative slope in our measurement range.

From the relationship in Fig. 6(b), we estimated the absorbance of the gelatin phantom with a 10% glucose concentration. Figure 7 shows the comparison between the measured absorbance using the ATR method and estimated absorbance using PZT-PAS. The estimated absorbance was performed by multiplying the value of the negative slope by the PA spectrum. As can be seen, because the spectral shapes of the two spectra are almost identical, it was found that the

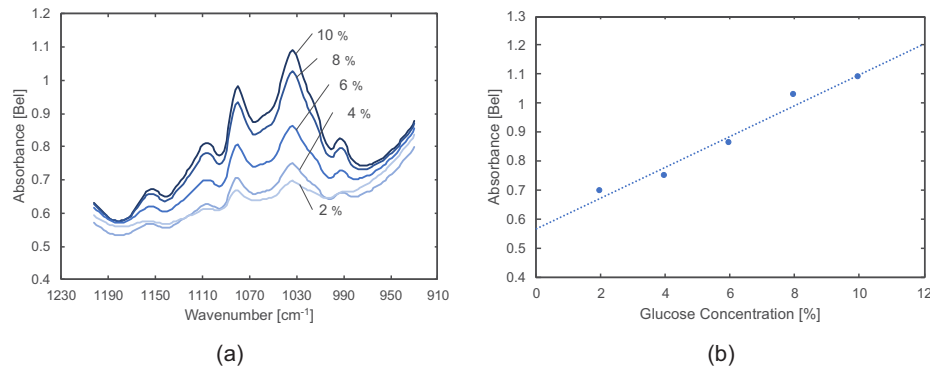


Fig. 5. ATR measurements of gelatin phantom with glucose: (a) ATR spectra of gelatin phantom with different glucose concentrations and (b) calibration curve for absorbance and glucose concentration.

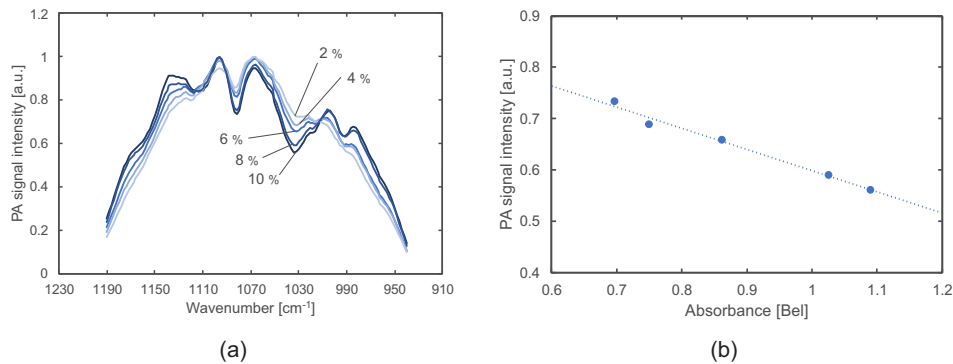


Fig. 6. PZT-PAS measurements of gelatin phantom with glucose: (a) PA spectra of gelatin phantom with different glucose concentrations and (b) Relationship between PA signal intensity and optical absorbance.

PA spectrum reflected the absorption characteristics of the sample, and the absorption spectrum could be estimated by PZT-PAS.

We then explored the current detection limits of the glucose concentration in our measurement system. Here, we prepared gelatin phantoms with different glucose concentrations of 0.1% and from 0.2% to 1%, with increments of 0.2%, and drew a calibration curve, as shown in Fig. 8. From this result, we confirmed the PZT-PAS system can detect glucose concentrations of 0.1% that is close to the blood glucose concentration in healthy subjects 0.1% (100 mg/dl) [14, 34].

3.2. Measurement with biological tissue and sensitivity improvement

We used the PZT-PAS system for biological tissue measurements using sliced poultry breast meat as a sample (Fig. 9 (a)). Figure 9 (b) shows the measured PA spectrum compared with the ATR spectrum. The error bars on the PZT-PAS spectrum show standard deviations of four measurements. The peaks and dips in the spectrum are not due to noise since their height and depth are larger enough than the magnitude of error bars. Figure 9 (c) shows the enlarged spectra from 1,030 cm⁻¹ to 1,170 cm⁻¹. As with the previous result, the PAS spectrum was almost inverted with respect to the ATR absorption spectrum. Although some wavenumber shifts exist, the absorption peaks appeared as dips in the PA spectrum. These peaks can be assigned to the

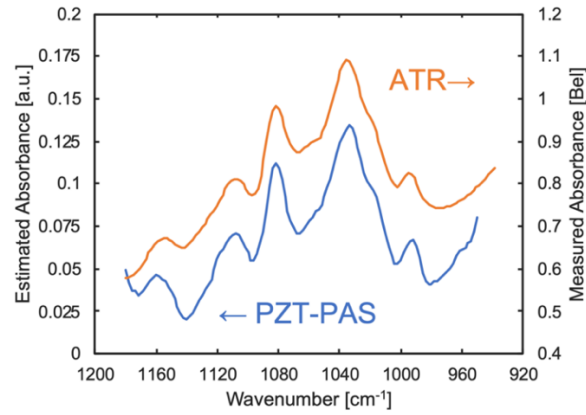


Fig. 7. Comparison between estimated absorbance from PZT-PAS and actual absorbance from ATR method.

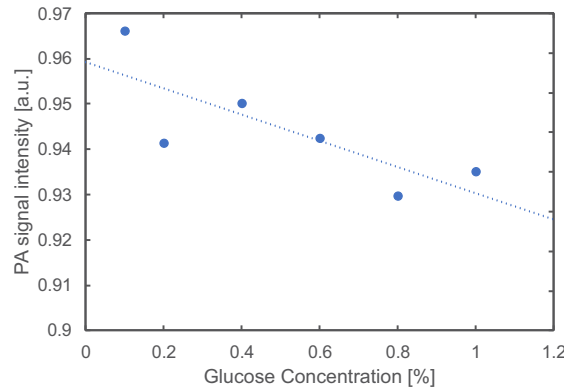


Fig. 8. The calibration curve for glucose concentration and PA signal intensity at $1,034\text{ cm}^{-1}$.

vibrational mode of the C-C stretch ($1,078\text{ cm}^{-1}$), C-O stretch of the ribose ring ($1,120\text{ cm}^{-1}$), and C-O stretch ($1,151\text{ cm}^{-1}$) [35], which are components of biological tissue or cells.

To further increase the measurement sensitivity, we performed signal intensity improvement for biological tissue analysis. The resonance vibration caused by standing waves originating from the induced ultrasound inside a sample was used to amplify the signal intensity. Standing waves are generated when incident and reflected waves interfere with each other. In our case, reflected waves are generated since the acoustic impedance gap between PZT transducer and sample is extremely large. For spherical waves generated from a wave source, we found that the signal enhancement effect due to the resonance appears only at the point where the distance from the wave source satisfies the resonance condition. We confirmed this by measuring the PA signal intensity that decreased when the PZT transducer was slightly moved to horizontal direction from resonance point. In this case, the sound pressure of the PA waves in the sample p is given as same as plane waves:

$$p = 2P|\cos(kz)| \quad (3)$$

where $P = \rho A$, ρ is the density of a sample, A is the amplitude of acoustic wave, k is the phase velocity in the sample, and z is the position ($z=0$ is the boundary surface between the PZT transducer and sample). Therefore, the amplitude of the acoustic pressure can be amplified when

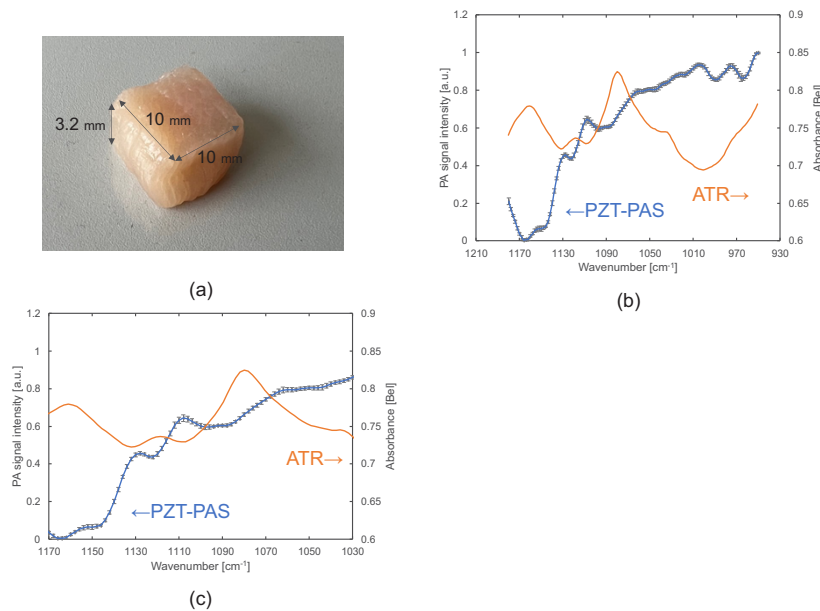


Fig. 9. Measurement of poultry meat: (a) appearance of the sample, (b) measured PA spectrum compared with ATR spectrum, and (c) enlarged spectra from $1,030\text{ cm}^{-1}$ to $1,170\text{ cm}^{-1}$. Error bars on PZT-PAS spectrum show standard deviations of four measurements.

the wavelength of acoustic wave is integer multiples of half wavelength, and the sample thickness is regulated to induce resonance vibration.

To confirm the phenomena in our experimental condition, a polyurethane gel pad (Sonagel, Takiron, Japan) (thickness = 5.0 mm) and poultry breast meat (thickness = 3.2 mm) were used as samples, and the results are shown in Figs. 10 (a) and (b), respectively. These results were obtained by pushing the PZT transducer onto the sample. For the spectra shown in Fig. 10 (a), we calculated the wavelength of induced ultrasound as $\lambda \sim 3.6\text{ mm}$ for 500 kHz and $\lambda \sim 3.0\text{ mm}$ for 600 kHz by using the sound speed in the polyurethane as 1,780 m/s. As can be observed in Fig. 10 (a), intensity peaks corresponding to integer multiples of half wavelength were observed. Similar to polyurethane gel pad, intensity peaks were observed in poultry breast meat, as shown in Fig. 10 (b). Although the peak points were not exactly matched with the expected thickness of 1.59 mm using the sound speed in the muscle tissue of 1,588 m/s [36], the signal intensity increased approximately tenfold at the intensity peaks. This slight difference in the peak position from the one expected might be caused by the density change of the sample when the transducer is pushed into the sample.

We then evaluated this resonance vibration effect with the poultry meat thickness between 1.6 mm and 4 mm. Figures 11(a) and 11(b) show the raw PA signal intensity spectra and PA spectra of a single scan, respectively. As can be observed, the signal intensity was amplified at the estimated resonance point owing to the improvement of the measurement sensitivity.

3.3. Measurement of the human earlobe

To apply resonance vibration by standing waves for measurements of human tissue, we chose the earlobe as the measurement part. Figure 12 shows a schematic of the earlobe measurement setup. The PZT transducer is located away from the laser beam, that is, the transducer is attached to the rear part of the sample, and its position can be changed to adjust the resonance vibration points. Because the diameter of the hole that makes contact with the earlobe is smaller than 2

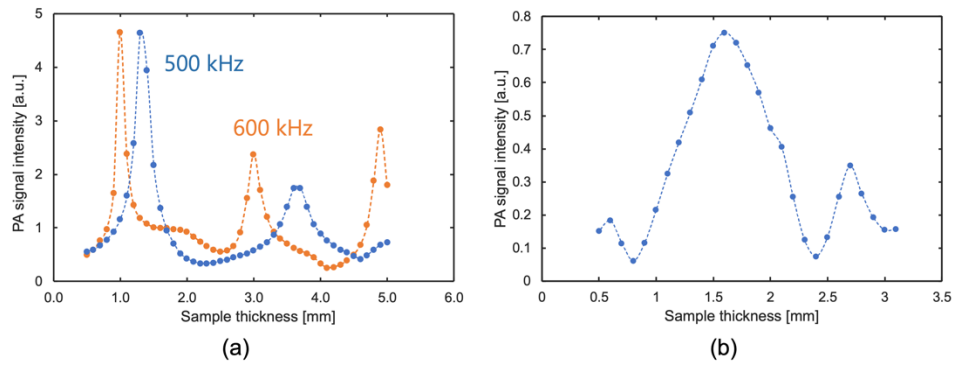


Fig. 10. Relationship between photoacoustic signal intensity and sample thickness: (a) polyurethane gel pad; (b) poultry breast meat

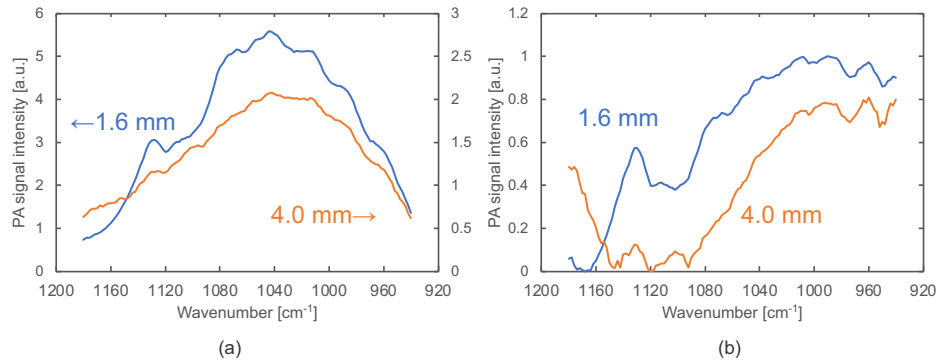


Fig. 11. Evaluation of resonance vibration effect: (a) raw PA signal intensity, (b) PA spectra

mm, the earlobe shape changes very little, even when adjusting the thickness, and does not affect the measurement data.

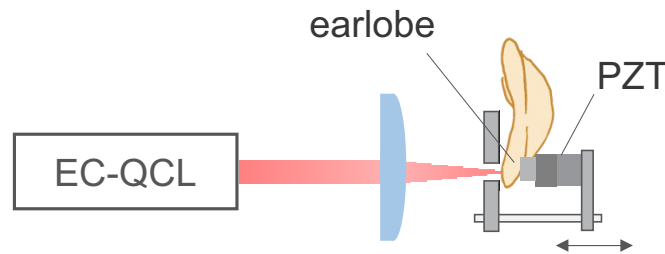


Fig. 12. Schematic of experimental setup for earlobe.

Figure 13(a) shows the spectra of the human earlobe obtained from the ATR method and PZT-PAS. For this measurement, the repetition frequency of the excitation light was set to 500 kHz. The sample thickness was adjusted to 2.9 mm to meet the sound wavelength in human tissue estimated from the speed of 1,440 m/s [36]. The error bars on the PZT-PAS spectrum show the standard deviations of four measurements. As shown in Fig. 13(b), the absorption peaks in the ATR at 1,030 cm⁻¹, 1,078 cm⁻¹, and 1,122 cm⁻¹ appear as dips in the PZT-PAS spectrum. The ATR and PZT-PAS spectra show different trends owing to the difference in the measurement

depths. Unlike the gelatin phantom, which is uniform in depth, biological tissue of different compositions varies in depth.

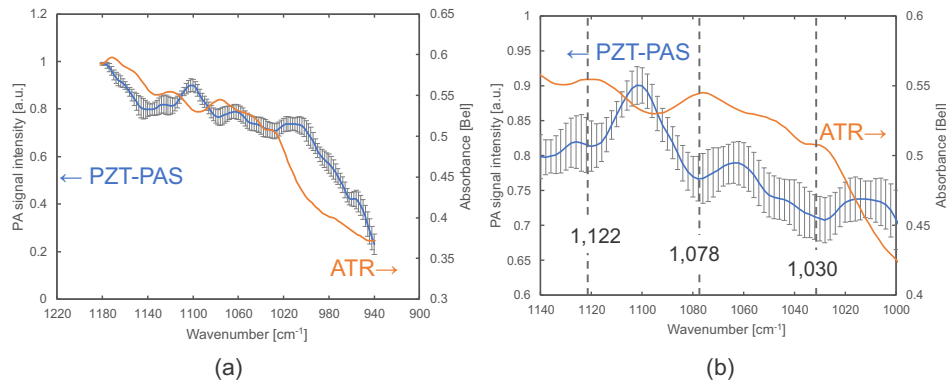


Fig. 13. Measured spectra of human earlobe: (a) whole measurement range, (b) enlarged figure from 1,000 cm^{-1} to 1,140 cm^{-1} . Error bars on PZT-PAS spectrum show standard deviations of four measurements.

In the measured spectrum, absorption peaks from the amino acid in the SC were observed at 1,075 cm^{-1} and 1,030 cm^{-1} [37]. In addition, the C-C stretch of glycogen at 1,078 cm^{-1} [35] and the absorption owing to lactate were also observed at 1,127 cm^{-1} [38]. Although more precise investigation to ascertain the contribution of the peaks is required using such as principal component analysis (PCA) and machine learning [39], the results indicate the potential of applying PZT-PAS to measure blood components. The intensity at 1,030 cm^{-1} is applicable to glucose detection, but another wavelength without absorption of glucose must be determined as a baseline [11].

4. Conclusions

We proposed and developed a PZT-PAS system for biological tissue analysis in the mid-infrared region as an alternative to the conventional microphone-PAS system. We found that the PA signal intensity obtained with this system was almost inversely proportional to the optical absorption, and that optical absorption peaks appeared as dips in the PZT-PAS spectra. From the results of the comparison between the PA signal intensity and optical absorption by using gelatin phantoms with different concentrations, we obtained a negative slope between them at 1,034 cm^{-1} of the absorption peak of the C-O stretch band of glucose. Furthermore, we confirmed that the PA spectrum reflected the absorption characteristics of the sample by utilizing the negative slope, indicating the possibility of spectroscopic analysis. The PZT-PAS system is able to discriminate vibrations as well as the FT-IR based ATR system. However, its measurement performance is limited and methods, such as principal component analysis (PCA) and machine learning, are needed to improve measurement performance. Further, a numerical study of the heat generation due to laser light absorption and the ultrasonic generation and propagation mechanism may be necessary to elucidate the piezoelectric-photoacoustic detection mechanism in the mid-infrared region, especially with regards to the relationship between the magnitude of the optical absorption and PA signal intensity of the samples.

Since the SNR of PZT-PAS is not sufficient compared to microphone-PAS, we further increased signal sensitivity of PZT-PAS by leveraging the resonance vibration of induced ultrasound. By adjusting the sample thickness and/or repetition frequency to the resonance vibration point, the signal intensity reached approximately tenfold, resulting in an increased SNR. To apply this effect to the *in skin* measurement, we chose the earlobe as the measurement part, and conducted its

measurement at the resonance vibration point. Some absorption dips corresponding to optical absorption peaks were clearly observed, including those originating from biological tissues or cells. Moreover, time-domain signal can be obtained if SNR is further improved. As a result, depth profile analysis may be possible.

The proposed PZT-PAS system represents a crucial step in non-invasive biological tissue analysis. Despite the non-linearity between the PA signal intensity and optical absorbance, we could observe PA spectra with several features attributed to the components in biological tissues. While this system may not be able to quantify the absorption properties of an object, multivariate analysis and machine-learning-based spectral analysis should be able to capture quantitative variations in the target component. In future studies, we will investigate the correlation of the PA spectra obtained from multiple subjects with specific blood components and attempt to estimate these components noninvasively.

Funding. Japan Society for the Promotion of Science (20H00231, 22K18785).

Disclosures. The authors declare no conflicts of interest directly relevant to the content of this article.

Data availability. Data underlying the results presented in this paper are not publicly available at this time but may be obtained from the authors upon reasonable request.

References

1. K. Ogurtsova, J.D. da Rocha Fernandes, Y. Huang, U. Linnenkamp, L. Guariguata, N.H. Cho, D. Cavan, J.E. Shaw, and L.E. Makaroff, "IDF Diabetes Atlas: Global estimates for the prevalence of diabetes for 2015 and 2040," *Diabetes Res. Clin. Pract.* **128**, 40–50 (2017).
2. C. F. So, K. S. Choi, T. K. S. Wong, and J. W. Y. Chung, "Recent advances in noninvasive glucose monitoring," *Med. Devices: Evidence Res.* **5**, 45–52 (2012).
3. T. Lin, A. Gal, Y. Mayzel, K. Horman, and K. Bahartan, "Non-invasive glucose monitoring: a review of challenges and recent advances," *Curr. Trends in Biomed. Eng. & Biosci.* **6**(5), 555696 (2017).
4. W. V. Gonzales, A. T. Mobashsher, and A. Abbosh, "The Progress of Glucose Monitoring—A Review of Invasive to Minimally and Non-Invasive Techniques, Devices and Sensors," *Sensors* **19**(4), 800 (2019).
5. M. Mita, I. Sugawara, K. Harada, M. Ito, M. Takizawa, K. Ishida, H. Ueda, T. Kitaguchi, and T. Tsuboi, "Development of red genetically encoded biosensor for visualization of intracellular glucose dynamics," *Cell Chem. Bio.* **29**(1), 98–108.e4 (2022).
6. N. Li, H. Zang, H. Sun, X. Jiao, K. Wang, T. C-Y Liu, and Y. Meng, "A non-invasive accurate measurement of blood glucose levels with raman spectroscopy of blood in microvessels," *Molecules* **24**(8), 1500 (2019).
7. S. Rassel, C. Xu, S. Zhang, and D. Ban, "Noninvasive blood glucose detection using a quantum cascade laser," *Analyst* **145**(7), 2441–2456 (2020).
8. V. P. Rachim and W. Chung, "Wearable-band type visible-near infrared optical biosensor for non-invasive blood glucose monitoring," *Sens. Actuators, B* **286**, 173–180 (2019).
9. Y. Tanaka, T. Tajima, M. Seyama, and K. Waki, "Differential continuous wave photoacoustic spectroscopy for non-invasive glucose monitoring," *IEEE Sens. J.* **20**(8), 4453–4458 (2020).
10. S. Liakat, K. A. Bors, T-Y Huang, Anna P. M. Michel, E. Zanghi, and C. F. Gmachl, "In vitro measurements of physiological glucose concentrations in biological fluids using mid-infrared light," *Biomed. Opt. Express* **4**(7), 1083–1090 (2013).
11. T. Koyama, S. Kino, and Y. Matsuura, "Accuracy improvement of blood glucose measurement system using quantum cascade lasers," *Opt. Photonics J.* **09**(10), 155–164 (2019).
12. T. Koyama, N. Shibata, S. Kino, A. Sugiyama, N. Akikusa, and Y. Matsuura, "A compact mid-infrared spectroscopy system for healthcare applications based on a wavelength-swept, pulsed quantum cascade laser," *Sensors* **20**(12), 3438 (2020).
13. M. A. Pleitez, T. Lieblein, A. Bauer, O. Hertzberg, H. von Lilienfeld-Toal, and W. Mäntele, "In vivo noninvasive monitoring of glucose concentration in human epidermis by mid-infrared pulsed photoacoustic spectroscopy," *Anal. Chem.* **85**(2), 1013–1020 (2013).
14. S. N. Thennadil, J. L. Rennert, B. J. Wenzel, K. H. Hazen, T. L. Ruchti, and M. B. Block, "Comparison of glucose concentration in interstitial fluid, and capillary and venous blood during rapid changes in blood glucose levels," *Diabetes Technol. Ther.* **3**(3), 357–365 (2001).
15. R. Kasahara, S. Kino, S. Soyama, and Y. Matsuura, "Noninvasive glucose monitoring using mid-infrared absorption spectroscopy based on a few wavenumbers," *Biomed. Opt. Express* **9**(1), 289–302 (2018).
16. H.D. Downing and D. Williams, "Optical constants of water in the infrared," *J. Geophys. Res.* **80**(12), 1656–1661 (1975).
17. M. Born and E. Wolf, *Principles of Optics: Electromagnetic Theory of Propagation, Interference and Diffraction of Light*, 7 th ed. (Cambridge University Press, 1999).

18. H. von Lilienfeld-Toal, M. Weidenmüller, A. Xhelaj, and W. Mänte, "A novel approach to non-invasive glucose measurement by mid-infrared spectroscopy: The combination of quantum cascade lasers (QCL) and photoacoustic detection," *Vib. Spectrosc.* **38**(1-2), 209–215 (2005).
19. J. Kottmann, J. M. Rey, J. Luginbühl, E. Reichmann, and M. W. Sigrist, "Glucose sensing in human epidermis using mid-infrared photoacoustic detection," *Biomed. Opt. Express* **3**(4), 667–680 (2012).
20. J. Kottmann, J. M. Rey, and M. W. Sigrist, "Mid-infrared photoacoustic detection of glucose in human skin: towards non-invasive diagnostics," *Sens.* **16**(10), 1663 (2016).
21. J. Kottmann, J. M. Rey, and M. W. Sigrist, "New photoacoustic cell design for studying aqueous solutions and gels," *Rev. Sci. Instrum.* **82**(8), 084903 (2011).
22. M. A. Pleitez, T. Lieblein, A. Bauer, O. Hertzberg, H. von Lilienfeld-Toal, and W. Mänte, "Windowless ultrasound photoacoustic cell for in vivo mid-IR spectroscopy of human epidermis: Low interference by changes of air pressure, temperature, and humidity caused by skin contact opens the possibility for a non-invasive monitoring of glucose in the interstitial fluid," *Rev. Sci. Instrum.* **84**(8), 084901 (2013).
23. T. Ishiguro and H. Tokumoto, "Application of Photoacoustic Spectroscopy to Solids," *Jpn. J. Appl. Phys.* **21**(S3), 11–15 (1982).
24. Y. H. El-Sharkawy, S. Elbasuney, A. El-sharif, M. Eltahlawy, and H.S. Ayoub, "Instantaneous identification of hazardous explosive-related materials using laser induced photoacoustic spectroscopy," *TrAC, Trends Anal. Chem.* **106**, 151–158 (2018).
25. F. C. Delori, R. H. Webb, and D. H. Sliney, "Maximum permissible exposures for ocular safety (ANSI 2000), with emphasis on ophthalmic devices," *J. Opt. Soc. Am. A* **24**(5), 1250–1265 (2007).
26. S. Kino, S. Omori, T. Katagiri, and Y. Matsuura, "Hollow optical-fiber based infrared spectroscopy for measurement of blood glucose level by using multi-reflection prism," *Biomed. Opt. Express* **7**(2), 701–708 (2016).
27. M. V. Korolevich, R. G. Zhabkov, and V. V. Sivchik, "Calculation of absorption band frequencies and intensities in the IR spectrum of α -D-glucose in a cluster," *J. Mol. Struct.* **220**(2), 301–313 (1990).
28. M. Ibrahim, M. Alaam, H. El-Haes, A. F. Jalbout, and A. de Leon, "Analysis of the structure and vibrational spectra of glucose and fructose," *Ecletica Quim.* **31**(3), 15–21 (2006).
29. W. Jackson and N. M. Amer, "Piezoelectric photoacoustic detection: theory and experiment," *J. Appl. Phys.* **51**(6), 3343–3353 (1980).
30. W.G. Spitzer and J. M. Whelan, "Infrared absorption and electron effective mass in n-type gallium arsenide," **114**(1), 59–63 (1959).
31. P. E. Dyer, "Laser ablation: Processes and applications," *Proc. SPIE* **3092**, 412 (1997).
32. J. A. Viator, S. L. Jacques, and S. A. Prahl, "Depth profiling of absorbing soft materials using photoacoustic methods," *IEEE J. Select. Topics Quantum Electron.* **5**(4), 989–996 (1999).
33. A. A. Oraevsky and S. L. Jacques, "Mechanism of laser ablation for aqueous media irradiated under confined-stress conditions," *J. Appl. Phys.* **78**(2), 1281–1290 (1995).
34. G. Greckmann, S. Hangenlocher, A. Baumstark, N. Jendrike, R. C. Gillen, K. Rössner, and C. Haug, "Continuous glucose profiles in healthy subjects under everyday life conditions and after different meals," *J. Diabetes Sci. Technol.* **1**(5), 695–703 (2007).
35. K. Malek, B. R. Wood, and K. R. Bamberg, "FTIR imaging of tissues: techniques and methods of analysis," *Optical Spectroscopy and Computational Methods in Biology and Medicine. Challenges and Advances in Computational Chemistry and Physics* **14**, 419–425 (Springer, 2014).
36. P. A. Hasgall, F. Di. Gennaro, C. Baumgartner, E. Neufeld, B. Lloyd, M. C. Gosselin, D. Payne, A. Klingenböck, and N. Kuster, "IT'IS Database for thermal and electromagnetic parameters of biological tissues," Ver.4.1 (2022).
37. P. Garidel, "Mid-FTIR-microspectroscopy of stratum corneum single cells and stratum corneum tissue," *Phys. Chem. Chem. Phys.* **4**(22), 5671–5677 (2002).
38. C. Petibois, A. M. Melin, A. Perromat, G. Cazorla, and G. Délérís, "Glucose and lactate concentration determination on single microsamples by Fourier-transform infrared spectroscopy," *J. Lab. Clin. Med.* **135**(2), 210–215 (2000).
39. A. Aloraynan, S. Rassel, C. Xu, and D. Ban, "A single wavelength mid-infrared photoacoustic spectroscopy for noninvasive glucose detection using machine learning," *Biosensors* **12**(3), 166 (2022).